

Simulating the nematic-isotropic phase transition of liquid crystal model via generalized replica-exchange method

Kengo Takemoto,¹ Yoshiki Ishii,² Hitoshi Washizu,² Kang Kim,^{1, a)} and Nobuyuki Matubayasi^{1, b)}

¹⁾*Division of Chemical Engineering, Graduate School of Engineering Science, Osaka University, Toyonaka, Osaka 560-8531, Japan*

²⁾*Graduate School of Information Science, University of Hyogo, Kobe, Hyogo 650-0047, Japan*

(Dated: 8 March 2024)

The nematic-isotropic (NI) phase transition of 4-cyano-4'-pentylbiphenyl (5CB) was simulated using the generalized replica-exchange method (gREM) based on molecular dynamics simulations. The effective temperature is introduced in gREM, allowing the enhanced sampling of configurations in the unstable region, which is intrinsic to the first-order phase transition. The sampling performance was analyzed with different system sizes and compared with that of the temperature replica-exchange method (tREM). It was observed that gREM is capable of sampling configurations at sufficient replica-exchange acceptance ratios even around the NI transition temperature. A bimodal distribution of the order parameter at the transition region was found, which is in agreement with the mean-field theory. In contrast, tREM is ineffective around the transition temperature owing to the potential energy gap between the nematic and isotropic phases.

I. INTRODUCTION

Highly anisotropic molecules can form a variety of mesophases, including nematic, smectic, and columnar phases between crystalline solids and isotropic liquids.¹ Such molecules exhibiting liquid crystal (LC) phases are referred to as mesogens. One of the common mesogens is 4-cyano-4'-pentylbiphenyl (5CB), which undergoes a nematic-isotropic (NI) phase transition at room temperature. An order parameter for characterizing the nematic LC phase is introduced with respect to the director, which is defined as a collection of mesogen molecules. The order parameter reduces with an increase in temperature. Typically, it reduces from 0.6 to 0.4 on approaching to the transition temperature and exhibits a discontinuous drop to zero at the transition. This behavior is regarded as a sign of the first-order phase transition, as demonstrated well by the mean-field theory for the NI transition.²⁻⁴

Because the time scale associated with the equilibration of the nematic phase becomes longer with an isotropic starting configuration, it is still challenging to perform molecular dynamics (MD) simulations of the NI phase transition from atomistic levels, even though considerable research has been conducted on the use of all-atom, united-atom (UA), and coarse-grained models.⁵⁻¹² In particular, MD simulations of systems exhibiting first-order phase transitions often encounter difficulties in sampling the configurations around the transition temperatures, owing to the presence of unstable states bridging the potential energy gaps between two stable phases.

The temperature replica-exchange method (tREM) (also known as parallel tempering) is a promising sampling method for simulating the phase transitions in various physical and chemical systems.^{13,14} The tREM is developed to sample a

wide range of configurations, where many replicas at different temperatures are simulated in parallel and the configurations between two replicas are exchanged to prevent replicas at lower temperatures from staying in the local minimum state. However, the exchanges of replicas become ineffective near the first-order phase transition temperature, which results in tREM inefficiency. It should be noted that various enhanced sampling methods beyond the original tREM have been developed.¹⁵ Berardi *et al.*¹⁶ and Kowaguchi *et al.*¹⁷ attempted to improve the sampling efficiency near the NI phase transition with the Gay-Berne model and anisotropic Lennard-Jones fluids using the multidimensional REM¹⁸ (also known as Hamiltonian REM¹⁹) and the isobaric-isothermal REM,²⁰ respectively.

Recently, Kim *et al.* proposed the generalized replica-exchange method (gREM),²¹ which was designed to efficiently simulate first-order phase transition systems. In gREM, the effective potential and effective temperature are introduced for each replica to ensure the unimodal distribution of the potential energy E of the system, even in the thermodynamically unstable region. The effective potential is derived from the ensemble weight, which is set to the Tsallis form in practical implementations. Further, by utilizing its dependence on the most probable value of E , the effective temperature is connected to the statistical temperature of the system. Sufficient overlaps were achieved for the probability distributions of E for replicas with different effective temperatures, which enabled efficient sampling of the transition region. The gREM has been applied to various systems showing solid-liquid^{22,23} and vapor-liquid^{24,25} transitions.

The isobaric extension of gREM was proposed by Małolepsza and Keyes.²⁶⁻²⁹ In this extension, the enthalpy H is used instead of the potential energy E , which is employed in the canonical case (to be exact, H refers to the sum of E and the product of pressure and volume). The effective temperature for each replica is introduced with respect to H , and owing to the use of H , gREM is appropriate for simulating constant-pressure ensembles. The isobaric gREM was also utilized

^{a)}Electronic mail: kk@cheng.es.osaka-u.ac.jp

^{b)}Electronic mail: nobuyuki@cheng.es.osaka-u.ac.jp

to investigate the liquid and vapor phases of water³⁰ and the order-disorder phase transitions in lipid bilayer systems.³¹

Therefore, it is of interest to assess the applicability of isobaric gREM to the NI phase transition, which is characterized by the orientational ordering. In this study, we performed MD simulations in combination with isobaric gREM for 5CB based on the united-atom (UA) model developed by Tiberio *et al.*³² Finite-size effects on the NI transition are important because an equilibration time scale near the phase transition region drastically increases with increasing the number of molecules N . In computer simulations for LC systems, the finite-size effects were indeed examined, for example, using the Lebwohl–Lasher model^{33–35} and anisotropic Lennard-Jones fluids.³⁶ We investigated system size effects by the use of gREM with the number of molecules N ranging from 250 to 4000. The sampling performance was also analyzed by comparison with tREM. From sampled configurations, we examine the temperature dependence of the density and order parameter and discuss the temperature and enthalpy relationship.

II. MODEL AND SIMULATION DETAILS

The UA model for 5CB developed by Tiberio *et al.* was utilized in this study. In this model, the generalized AMBER force field (GAFF) was modified to reproduce the temperature of the NI phase transition in the experiments, $T_{\text{NI}} \approx 308.2$ K.³² The comparison with experimental results of the density and order parameter was also reported in Ref. 32. This UA model has also been employed in previous studies,^{37–39} which considered the NI phase transition in a consistent manner with Ref. 32. Another UA model was developed by the parametrization of the TraPPE-UA force field for the 5CB molecule.⁴⁰ Moreover, the transferability of the coarse-grained model has also been proposed.^{41,42} The present work is mainly methodological, and Tiberio *et al.*'s model was employed since it reflects the chemical reality and reproduces the NI transition temperature well.

The simulated system was composed of 5CB molecules in a cubic box with periodic boundary conditions. The number of molecules was varied as $N = 250, 1000, 2000$, and 4000. The pressure was set to 1 atm, and the temperatures were ranged between 300 K and 320 K. The *NPT* ensemble with the N ose–Hoover thermostat and isotropic Parrinello–Rahman barostat was used with a time step of 2 fs in all the simulations. We performed gREM and tREM using the Large-scale Atomic/Molecular Massively Parallel Simulator (LAMMPS)⁴³.

The basic idea of gREM is summarized as follows (see the detail in Ref. 21): The effective temperature T_α of replica α ($=1, 2, \dots, M$) is introduced by an inverse mapping of the effective potential w_α , $T_\alpha = (\partial w_\alpha / \partial E)^{-1}$. w_α is related to the ensemble weight W_α through the relation, $w_\alpha = -\ln W_\alpha$. T_α is set to intersect the statistical temperature, $T_s = (\partial S / \partial E)^{-1}$. Here, S and E denote the configurational entropy and potential energy in the canonical ensemble, respectively. Furthermore, the parametrization with a linear function for the effective

TABLE I. Enthalpy at 300 K and 320 K (denoted by \tilde{H}_1 and \tilde{H}_M for the use of gREM, respectively), and slope γ for the gREM at the examined system sizes. The enthalpy is normalized by the number of molecules N .

N	250	1000	2000	4000
\tilde{H}_1/N (kcal·mol ⁻¹)	69.4	69.4	69.5	69.4
\tilde{H}_M/N (kcal·mol ⁻¹)	71.9	71.9	71.9	71.9
γ (10 ⁻³ K/kcal·mol ⁻¹)	-31.9	-8.14	-4.11	-2.04

temperature, $T_\alpha(E) = \lambda_\alpha + \gamma(E - E_0)$, provides the ensemble weight that is equivalent with the form of the Tsallis statistics, $W_\alpha \sim [\lambda_\alpha + \gamma(E - E_0)]^{-1/\gamma}$. Here, E_0 represents an arbitrarily chosen potential energy and γ is chosen to have a sufficiently large negative value to ensure that $T_\alpha(E)$ intersects $T_s(E)$ only once. Note that λ_α is a control parameter for determining the distribution of E in replica α for a given slope γ . The non-Boltzmann ensemble with the weight W_α and effective temperature T_α enables to sample the thermodynamically unstable states bridging two stable phases.

The isobaric gREM is formalized considering the enthalpy H , statistical temperature $T_s = (\partial S / \partial H)^{-1}$, and effective temperature $T_\alpha = (\partial w_\alpha / \partial H)^{-1}$ for replica α .²⁶ In isobaric gREM, the enthalpy dependent effective temperature for replica α is given by

$$T_\alpha(H) = \lambda_\alpha + \gamma(H - H_0), \quad (1)$$

where H is the sum of the potential energy and the product of pressure and volume, and H_0 and γ represent the reference enthalpy and the slope of $T_\alpha(H)$, respectively. Again, γ and λ_α are control parameters of the temperature intercept at a chosen enthalpy H_0 . The acceptance probability of replica exchange between neighboring replicas α (with enthalpy H) and α' (with enthalpy H') is given by

$$A_{\alpha,\alpha'} = \min[1, \exp(\Delta_{\alpha,\alpha'})], \quad (2)$$

with $\Delta_{\alpha,\alpha'} = w_{\alpha'}(H') - w_{\alpha'}(H) + w_\alpha(H) - w_\alpha(H')$. In contrast, the acceptance of replica exchange in tREM is given by Eq. (2) with $\Delta_{\alpha,\alpha'} = (\beta_\alpha - \beta_{\alpha'})(E_\alpha - E_{\alpha'})$, where $\beta_\alpha = 1/T_\alpha$ and $\beta_{\alpha'} = 1/T_{\alpha'}$ are inverse temperatures of replica α and α' , respectively. The volume is equilibrated with the barostat of 1 atm if the replica exchange is occurred.

In the present simulations, $M = 11$ replicas were utilized for both gREM and tREM. The lowest and highest temperatures were 300 K and 320 K; hence, temperatures of replicas 1 and M were $T_1 = 300$ K and $T_M = 320$ K, respectively. The values of enthalpy at the two temperatures (denoted by \tilde{H}_1 and \tilde{H}_M , respectively) were quantified from the averages of 10 ns simulations after equilibration over 50 ns using the *NPT* ensemble. For supplementary comparison, we also simulated isobaric-isothermal REM by Okabe *et al.*²⁰ with $N = 4000$, where $\Delta_{\alpha,\alpha'} = (\beta_\alpha - \beta_{\alpha'})(E_\alpha - E_{\alpha'}) + (\beta_\alpha p_\alpha - \beta_{\alpha'} p_{\alpha'})(V_\alpha - V_{\alpha'})$ is used in Eq. (2) with the pressure and volume pairs (p_α, V_α) and $(p_{\alpha'}, V_{\alpha'})$ of replica α and α' , respectively. The second term is designed to employ the enthalpic quantity for generation of an isobaric-isothermal ensemble.

For gREM, the slope γ was determined from $\gamma = (T_M - T_1)/(\tilde{H}_1 - \tilde{H}_M)$. The values of \tilde{H}_1 , \tilde{H}_M , and γ are listed in Table I. The reference enthalpy H_0 in Eq. (1) was set to \tilde{H}_1 in the present gREM. It is also seen that \tilde{H}_1/N and \tilde{H}_M/N are insensitive to the system size; therefore, γ varies roughly in inverse proportion to N . The control parameter λ_α for replica α is given by $\lambda_\alpha = \lambda_1 + \Delta\lambda(\alpha - 1)$ with $\Delta\lambda = (\lambda_M - \lambda_1)/(M - 1)$, where $\lambda_1 = T_1$ and $\lambda_M = T_M - \gamma(\tilde{H}_M - \tilde{H}_1)$. In contrast, for tREM, the temperature of replica α is given by $T_\alpha = T_1 + \Delta T(\alpha - 1)$ with $\Delta T = 2$ K. A 50 ns simulation was run, in which a temperature swap between adjacent replicas were attempted every 10 ps both for both gREM and tREM. We calculated various quantities presented in Sec. III from the last 10 ns simulation containing 1000 configurations, where the stationary state was achieved. Since all the events of temperature swap were tracked, the data can be extracted for each replica in both gREM and tREM.

Note that the most probable enthalpy H^* in gREM provides the relation, $T_s = T_\alpha(H^*)$.²⁶ Henceforth, T of gREM is represented by the temperature determined from the peak of the enthalpy distribution for each replica from Eq. (1) (see also Fig. 4(a) below). In contrast, T of tREM is represented by the designed temperature of each replica.

III. RESULTS AND DISCUSSION

First, we investigate the temperature dependence of the density. Figure 1 shows the results for gREM (a) and tREM (b) by changing the number of molecules N . The sudden drop of the density is evident at around 305-310 K, particularly for the larger system size with $N = 4000$. The transition from nematic to isotropic phases occurs in this temperature range, as demonstrated in previous studies using the same UA model.^{32,37-39}

We next examine the orientational order parameter of the LC nematic phase. The order parameter P_2 is generally expressed by the second-order Legendre polynomial as follows:

$$P_2 = \left\langle \frac{1}{N} \sum_{i=1}^N \left(\frac{3}{2} \cos^2 \theta_i - \frac{1}{2} \right) \right\rangle, \quad (3)$$

where θ_i represents the angle between the director \mathbf{n} and the unit vector of the long axis of molecular i , \mathbf{u}_i . Here, the director \mathbf{n} is the unit vector representing the preferred direction of the local volume. The brackets denote the an ensemble averages. The most widely used method to quantify P_2 from MD simulations is the diagonalization of the order parameter tensor \mathbf{Q} .^{44,45} The expression of \mathbf{Q} is given by

$$\mathbf{Q} = \left\langle \frac{1}{N} \sum_{i=1}^N \left(\frac{3}{2} \mathbf{u}_i \otimes \mathbf{u}_i - \frac{1}{2} \mathbf{I} \right) \right\rangle, \quad (4)$$

with the unit matrix \mathbf{I} . The eigenvalues of the matrix \mathbf{Q} , $\lambda_- < \lambda_0 < \lambda_+$, guarantee $\lambda_- + \lambda_0 + \lambda_+ = 0$ because \mathbf{Q} is traceless. The largest eigenvalue λ_+ provides the order parameter P_2 , and the corresponding eigenvector is the director \mathbf{n} . In practice, P_2 was calculated as $-2\lambda_0$, which was suggested for

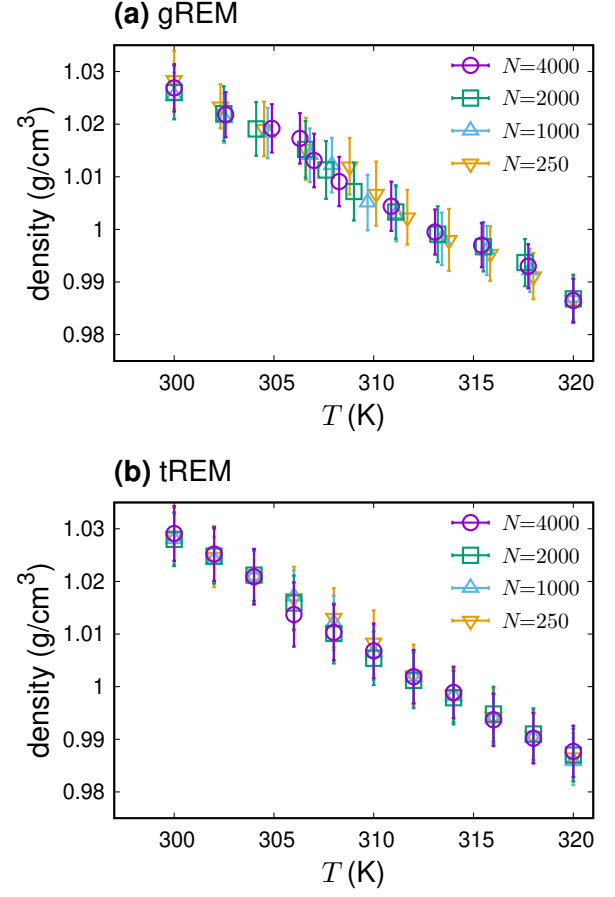


FIG. 1. Temperature dependence of the average of density with different system sizes $N = 250, 1000, 2000$, and 4000 , using the gREM (a) and tREM (b). The bar associated with each point of the density corresponds to the standard deviation.

a better estimation of P_2 , particularly in the isotropic phase.⁴⁶ Here, \mathbf{u}_i in this work refers to the C≡N bond of the cyano group. Note that the dependence of the choice of \mathbf{u}_i on P_2 was negligible if the inertia axis of the molecule is used.³²

Figure 2 shows the temperature dependence of the order parameter P_2 from gREM (a) and tREM (b) simulations. It is observed that the decrease in temperature T leads to a decrease in P_2 from 0.5-0.6 to nearly zero for all the system sizes that were investigated. The temperature dependence of P_2 exhibits a sharper drop across the NI transition for the larger system with $N = 4000$. However, P_2 for the smallest system size with $N = 250$ gradually decreases with increasing T . In general, the discontinuity of the first-order phase transition between two stable states are smeared out in finite systems.^{47,48} The N dependence in Fig. 2 is in accordance with the well-known fact that unstable regions of the phase transition become narrow as the system size decreases.

Here, we used the empirical equation,^{49,50}

$$P_2 = (1 - P_2^{\text{iso}}) \left(1 - \frac{T}{T_{\text{NI}}} \right)^\beta + P_2^{\text{iso}}, \quad (5)$$

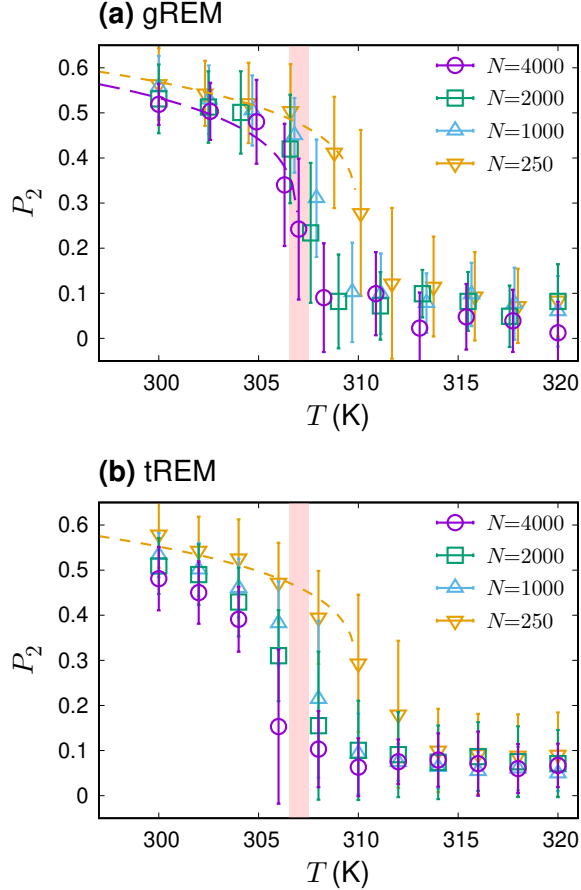


FIG. 2. Temperature dependence of the average of the order parameter P_2 with different system sizes $N = 250, 1000, 2000$, and 4000 , using the gREM (a) and tREM (b). The bar associated with each point of P_2 corresponds to the standard deviation. In (a), the purple dashed curve represents the fitting result with Eq. (5) for $N = 4000$. The vertical bar indicates the NI transition temperature, $T_{NI} \approx 307$ K, determined from the fitting for results of $N = 4000$. In (a) and (b), the fitting results with Eq. (5) for $N = 250$ are described by the orange dashed curves. The NI transition temperature is $T_{NI} \approx 310$ K, which is consistent with the value reported in Ref. 32.

for fitting with the order parameter P_2 . We obtained the residual order parameter under the isotropic phase $P_2^{iso} \approx 0.12$, NI transition temperature $T_{NI} \approx 307$ K, and pseudo-critical exponent $\beta \approx 0.20$ for the gREM result with $N = 4000$. The fitting result is shown in Fig. 2(a). Note that $T_{NI} \approx 307$ K is slightly lower than the experimental value of 308 K.^{51,52} In contrast, the fitting for tREM with $N = 4000$ becomes uncertain due to the unsampled value of P_2 around the NI transition temperature, as observed in Fig. 2(b). The fittings of P_2 with $N = 250$ using Eq. (5) are also shown in Fig. 2 (a) and (b). For both gREM and tREM, the NI transition temperature is estimated as $T_{NI} \approx 310$ K. This value is in good agreement with the NI temperature reported in Ref. 32, where the number of molecules was $N = 250$. Furthermore, $\beta \approx 0.23$ (gREM) and $\beta \approx 0.21$ (tREM) are also close to the reported value of 0.226.³²

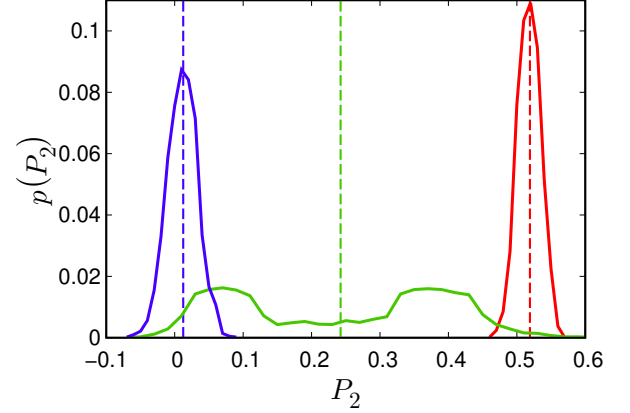


FIG. 3. Probability distribution of the order parameter P_2 sampled in replicas 1 (blue), 5 (green), and 11 (red) using the gREM with $N = 4000$. Their effective temperatures are 320, 307.0, and 300 K, respectively. The vertical lines indicate the mean values, *i.e.*, $P_2 \approx 0.02$ (blue), 0.26 (green), and 0.52 (red).

The distribution of the orientational order parameter P_2 is also important to examine the NI transition.³² Figure 3 shows the results from replicas 1, 5, and 11 for the gREM with $N = 4000$. The corresponding temperatures $T_\alpha(H^*)$ of gREM are 300 K, 307.0 K, and 320 K, respectively. The value of 307.0 K corresponds to T_{NI} , which was determined from the fitting results using Eq. (5). The distributions of P_2 in replicas 1 and 10 are unimodal, whereas two peaks at $P_2 \approx 0.1$ and 0.4 are observed in replica 5, resulting in the large fluctuation of P_2 at 307.0 K, as shown in Fig. 2(a). The bimodal distribution of the order parameter P_2 is consistent with the free energy landscape predicted by the mean-field theory for first-order phase transitions¹. However, the theoretical exponent $\beta = 0.5$ is different from the simulation result. In addition, it is interesting to examine pretransitional behaviors in the isotropic phase because the NI transition is relatively weak first-order phase transition. This regard can be characterized by the short-ranged orientational order from the orientational correlation functions $G_1(r) = \langle \delta(r - r_{ij})(\mathbf{u}_i \cdot \mathbf{u}_j) \rangle_{ij}$ and $G_2(r) = \langle \delta(r - r_{ij})[(3/2)(\mathbf{u}_i \cdot \mathbf{u}_j)^2 - (1/2)] \rangle_{ij}$,³² where r_{ij} denotes the distance of center-of-mass between molecules i and j . We also calculated $G_1(r)$ and $G_2(r)$ using the gREM with $N = 4000$ and obtained results consistent with those reported in Ref. 32 (data not shown).

It should be noted that the difference between gREM and tREM becomes significant for the system with $N = 4000$ around T_{NI} (see Figs. 1 and 2). Although the reduction of density and P_2 with temperature was also reproduced using the tREM, the values of density and P_2 from the tREM and gREM were not in agreement in the transition region. In particular, the averaged P_2 at 306 K (replica 4) of the tREM in Fig. 2(b) is close to the value in the isotropic phase with a large error bar. To elucidate the difference between the tREM and gREM with $N = 4000$, we quantified the acceptance ratios of the replica exchanges, the results of which are sum-

TABLE II. Acceptance ratio of the replica exchanges during the last 10 ns simulation between two replicas α and $\alpha + 1$ for the gREM and tREM with $N = 4000$. Note that * indicates that no exchanges were observed during 1000 trials.

replica index α	1	2	3	4	5	6	7	8	9	10
gREM (%)	14.8	13.6	12.8	12.9	12.5	14.6	17.4	18.1	18.3	18.9
tREM (%)	8.0	4.8	6.0	0.8	*	3.2	5.2	11.6	7.2	11.4

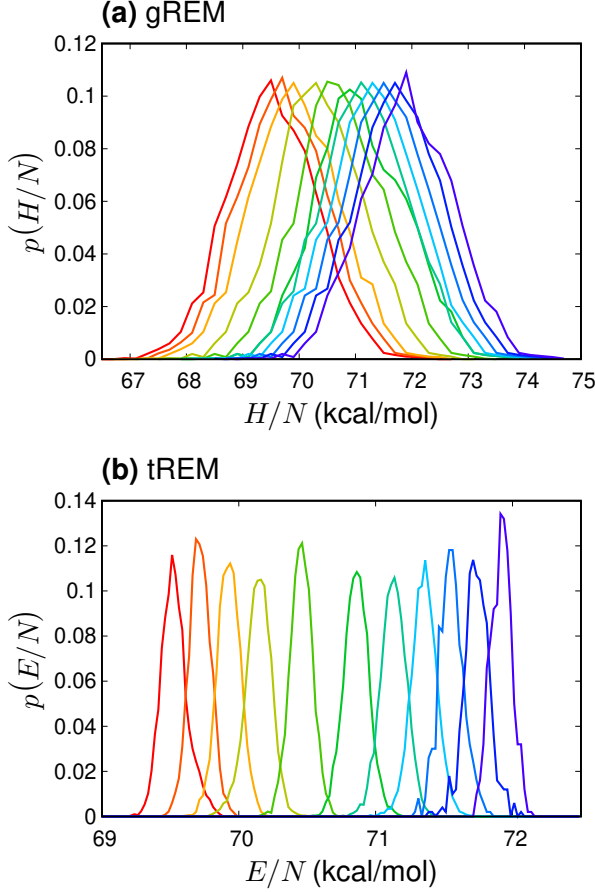


FIG. 4. Probability distributions of enthalpy H and potential energy E for different replicas of the gREM (a) and tREM (b) with $N = 4000$. From left to right, the replica index α ranges from 1 to 11. The enthalpy and potential energy are normalized by the number of molecules N .

marized in Table II. The acceptance ratio in gREM is larger than that in tREM for any pair of replica exchanges. The exchange ratio in gREM reduces between replicas 4 and 5, near $T_{\text{NI}} \approx 307$ K. Nevertheless, it exceeds 10% and assures the efficiency of the replica-exchange method. This is clear evidence that gREM is an effective simulation method, even near the phase transition temperature for larger system sizes. By contrast, the replica exchanges between replicas 4 ($T = 306$ K) and 5 ($T = 308$ K) and between replicas 5 ($T = 308$ K) and 6 ($T = 310$ K) are significantly restricted in tREM, which is an effect of the phase transition, as anticipated beforehand. We confirmed that the isobaric-isothermal REM relatively en-

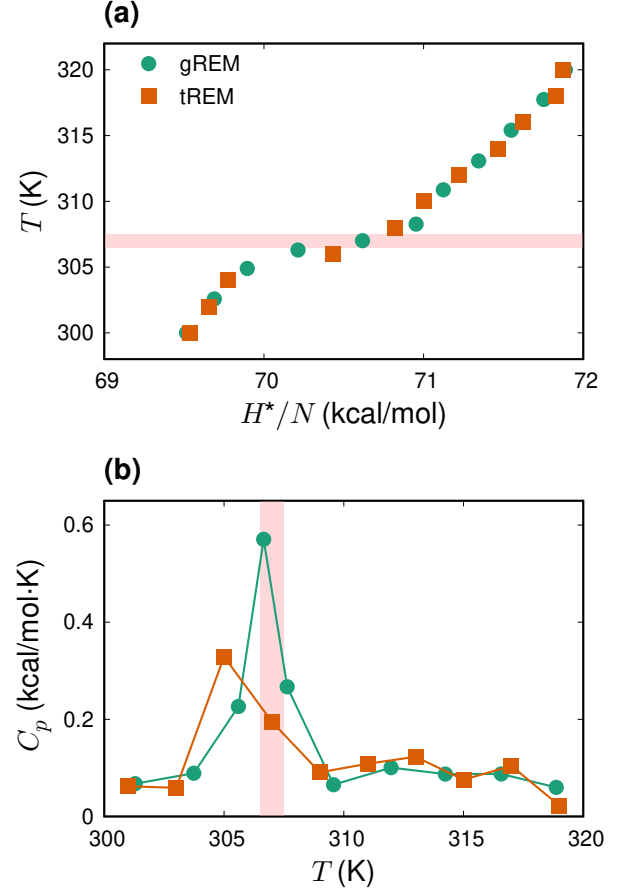


FIG. 5. (a) The temperature T as a function of the normalized enthalpy H^*/N for gREM and tREM with $N = 4000$. H^* represents the most probable enthalpy for each replica, resulting in the statistical temperature T from the relation $T_\alpha(H^*)$ for gREM. For tREM, T represents the designed temperature of each replica. From left to right, the replica index α ranges from 1 to 11. (b) Heat capacity C_p as a function of temperature T for gREM and tREM with $N = 4000$. The horizontal bar in (a) and the vertical bar in (b) indicate the NI transition temperature, $T_{\text{NI}} \approx 307$ K, respectively.

hances the replica exchange between neighboring replicas, but the acceptance ratio between replicas 4 and 5 remains small at 0.2%. This is due to the fact that the volume change of the NI transition is small about 4% from 300 K to 320 K (see Fig. 1).

The acceptance ratios between neighboring replicas are determined by the degree of overlap in the enthalpy or potential energy distributions in gREM or tREM, respectively. Figure 4 shows the probability distribution of enthalpy in gREM (a)

and potential energy in tREM (b) for each replica. The transition region corresponds to replicas 4, 5, and 6. The overlap of the distributions is significant in this region when gREM is employed. However, the overlap becomes scarce when using tREM, leading to a significant reduction in replica-change events. In principle, the acceptance ratios of replica exchanges in tREM can be improved by using more replicas to increase the degree of overlap of the potential energy distribution. However, simulating the tREM with more replicas is impractical in terms of computational costs, particularly for significantly larger system sizes. In contrast, for the smallest system size with $N = 250$, we confirmed that replica exchanges of tREM remain even at the NI transition region, showing behaviors in the density and P_s similar to those of gREM, as seen in Figs. 1 and 2.

Finally, we examine the relationship between the temperature T and most probable enthalpy H^* , which is plotted in Fig. 4(a). Here, T of gREM was determined from $T_s = T_\alpha(H^*)$ using Eq. (1) with the peak value H^* of the enthalpy distribution for replica α (see Fig. 4(a)). It has been demonstrated that T becomes flat when crossing the NI transition temperature ($T_{\text{NI}} \approx 307$ K). For comparison, the temperature as a function of H^* from tREM simulations with $N = 4000$ is also shown in Fig. 5(a). Although $T(H^*)$ of tREM also exhibits a curve similar to that of gREM, the plotted points become sparse, particularly for the NI transition region. The temperature dependence of the heat capacity $C_p = \partial(H^*/N)/\partial T$ with $N = 4000$ can be further evaluated from a central difference approximation for H^*/N as a function of T , as plotted in Fig. 5(b). The sharp peak associated with the NI phase transition was observed at $T_{\text{NI}} \approx 307$ K for gREM. This peak is also consistent with the drop of the density at the NI transition with $N = 4000$, as observed in Fig. 1(a). In contrast, the peak of C_p becomes unclear for tREM, again indicating the necessity of more replicas to increase the resolution around the NI transition. For smaller system sizes, the inflection of the $T - H^*/N$ curve is gradually smeared out, causing smaller peaks of C_p for both gREM and tREM (data not shown).

IV. CONCLUSIONS

In this paper, we report on MD simulation results combined with the gREM for the NI phase transition of the 5CB model. We demonstrated that the gREM can be applied to the NI phase transition of LC systems. It is effective in the sense that the acceptance ratios of the replica exchange remain significant at the NI transition temperature even with increasing N . By contrast, the replica exchange of tREM became inefficient, particularly for larger system sizes, although tREM simulated the results similar to those with gREM for $N = 250$.

The temperature dependence of the density and orientational order parameter P_2 was also examined. In particular, P_2 in the transition region between the nematic and isotropic phases can be sampled well using the gREM with the help of the effective temperature. A sharp drop in P_2 toward the NI temperature was observed, and this was more prominent for

larger system sizes. In addition, a sharp peak of heat capacity C_p was clearly observed around the NI temperature.

An advantage of gREM is its availability for the smectic phase of 4-octyl-4'-cyanobiphenyl (8CB) using the relevant UA model.⁵³ Note that a recent work shows the free energy landscape of smectic-nematic phase transition using machine learning technique.⁵⁴ It is interesting to examine these complex phase transition behaviors using gREM. Moreover, it is important to investigate the applicability of gREM in all-atom MD simulations of LC systems, for example, self-assembling helical structures⁵⁵ and nanochannels,⁵⁶ where phase transitions occur continuously over a wide temperature range. Further studies focusing on these aspects are required.

ACKNOWLEDGMENTS

The authors acknowledge Prof. Go Watanabe of Kitasato University for helpful discussions. K.K. is grateful to Prof. Hajime Yoshino of Osaka University for valuable comments. This work was supported by JSPS KAKENHI Grant Numbers: JP19H05718 (H.W.), JP18H01188 (K.K.), JP19H01812 (K.K.), JP20H05221 (K.K.), and JP19H04206 (N.M.). This work was also partially supported by the Fugaku Supercomputing Project (No. JPMXP1020200308) and the Elements Strategy Initiative for Catalysts and Batteries (No. JPMXP0112101003) from the Ministry of Education, Culture, Sports, Science, and Technology. The numerical calculations were performed at Research Center of Computational Science, Okazaki Research Facilities, National Institutes of Natural Sciences, Japan.

AUTHOR DECLARATIONS

CONFLICTS OF INTEREST

The authors have no conflicts to disclose.

DATA AVAILABILITY

The data that support the findings of this study are available from the corresponding authors upon reasonable request.

¹P. G. de Gennes and J. Prost, *The Physics of Liquid Crystals*, 2nd ed. (Oxford University Press, Oxford, 1995).

²M. J. Stephen and J. P. Straley, "Physics of liquid crystals," *Rev. Mod. Phys.* **46**, 617–704 (1974).

³S. Singh, "Phase transitions in liquid crystals," *Phys. Rep.* **324**, 107–269 (2000).

⁴D. Andrienko, "Introduction to liquid crystals," *J. Mol. Liq.* **267**, 520–541 (2018).

⁵C. Zannoni, "Molecular design and computer simulations of novel mesophases," *J. Mater. Chem.* **11**, 2637–2646 (2001).

⁶C. M. Care and D. J. Cleaver, "Computer simulation of liquid crystals," *Rep. Prog. Phys.* **68**, 2665–2700 (2005).

⁷M. R. Wilson, "Progress in computer simulations of liquid crystals," *Int. Rev. Phys. Chem.* **24**, 421–455 (2005).

- ⁸M. R. Wilson, "Molecular simulation of liquid crystals: progress towards a better understanding of bulk structure and the prediction of material properties," *Chem. Soc. Rev.* **36**, 1881 (2007).
- ⁹R. Berardi, L. Muccioli, S. Orlandi, M. Ricci, and C. Zannoni, "Computer simulations of biaxial nematics," *J. Phys.: Condens. Matter* **20**, 463101 (2008).
- ¹⁰S. Bag, S. Saurabh, Y. Lansac, and P. K. Maiti, "Atomistic and Coarse-Grained Simulation of Liquid Crystals," in *Self-Assembling Systems: Theory and Simulation*, edited by L.-T. Yan (Wiley, West Sussex, 2016) pp. 320–352.
- ¹¹C. Zannoni, "From idealised to predictive models of liquid crystals," *Liq. Cryst.* **45**, 1880–1893 (2018).
- ¹²M. P. Allen, "Molecular simulation of liquid crystals," *Mol. Phys.* **117**, 2391–2417 (2019).
- ¹³K. Hukushima and K. Nemoto, "Exchange Monte Carlo Method and Application to Spin Glass Simulations," *J. Phys. Soc. Jpn.* **65**, 1604–1608 (1996).
- ¹⁴Y. Sugita and Y. Okamoto, "Replica-exchange molecular dynamics method for protein folding," *Chem. Phys. Lett.* **314**, 141–151 (1999).
- ¹⁵Y. Okamoto, "Generalized-ensemble algorithms: enhanced sampling techniques for Monte Carlo and molecular dynamics simulations," *J. Mol. Graph. Model.* **22**, 425–439 (2004).
- ¹⁶R. Berardi, C. Zannoni, J. S. Lintuvuori, and M. R. Wilson, "A soft-core Gay-Berne model for the simulation of liquid crystals by Hamiltonian replica exchange," *J. Chem. Phys.* **131**, 174107 (2009).
- ¹⁷A. Kowaguchi, P. E. Brumby, and K. Yasuoka, "Phase Transitions and Hysteresis for a Simple Model Liquid Crystal by Replica-Exchange Monte Carlo Simulations," *Molecules* **26**, 1421 (2021).
- ¹⁸Y. Sugita, A. Kitao, and Y. Okamoto, "Multidimensional replica-exchange method for free-energy calculations," *J. Chem. Phys.* **113**, 6042–6051 (2000).
- ¹⁹H. Fukunishi, O. Watanabe, and S. Takada, "On the Hamiltonian replica exchange method for efficient sampling of biomolecular systems: Application to protein structure prediction," *J. Chem. Phys.* **116**, 9058–9067 (2002).
- ²⁰T. Okabe, M. Kawata, Y. Okamoto, and M. Mikami, "Replica-exchange Monte Carlo method for the isobaric–isothermal ensemble," *Chem. Phys. Lett.* **335**, 435–439 (2001).
- ²¹J. Kim, T. Keyes, and J. E. Straub, "Generalized Replica Exchange Method," *J. Chem. Phys.* **132**, 224107 (2010).
- ²²Q. Lu, J. Kim, and J. E. Straub, "Exploring the Solid–Liquid Phase Change of an Adapted Dzugutov Model Using Generalized Replica Exchange Method," *J. Phys. Chem. B* **116**, 8654–8661 (2012).
- ²³Q. Lu, J. Kim, J. D. Farrell, D. J. Wales, and J. E. Straub, "Investigating the solid-liquid phase transition of water nanofilms using the generalized replica exchange method," *J. Chem. Phys.* **141**, 18C525 (2014).
- ²⁴Q. Lu, J. Kim, and J. E. Straub, "Order parameter free enhanced sampling of the vapor-liquid transition using the generalized replica exchange method," *J. Chem. Phys.* **138**, 104119 (2013).
- ²⁵D. Ballal, Q. Lu, M. Raju, and X. Song, "Studying vapor-liquid transition using a generalized ensemble," *J. Chem. Phys.* **151**, 134108 (2019).
- ²⁶E. Małolepsza, M. Secor, and T. Keyes, "Isobaric Molecular Dynamics Version of the Generalized Replica Exchange Method (gREM): Liquid–Vapor Equilibrium," *J. Phys. Chem. B* **119**, 13379–13384 (2015).
- ²⁷E. Małolepsza and T. Keyes, "Water Freezing and Ice Melting," *J. Chem. Theory Comput.* **11**, 5613–5623 (2015).
- ²⁸E. Małolepsza, J. Kim, and T. Keyes, "Entropic Description of Gas Hydrate Ice–Liquid Equilibrium via Enhanced Sampling of Coexisting Phases," *Phys. Rev. Lett.* **114**, 170601 (2015).
- ²⁹E. Małolepsza and T. Keyes, "Pathways through Equilibrated States with Coexisting Phases for Gas Hydrate Formation," *J. Phys. Chem. B* **119**, 15857–15865 (2015).
- ³⁰W. J. Cho, J. Kim, J. Lee, T. Keyes, J. E. Straub, and K. S. Kim, "Limit of Metastability for Liquid and Vapor Phases of Water," *Phys. Rev. Lett.* **112**, 157802 (2014).
- ³¹D. Stelter and T. Keyes, "Enhanced Sampling of Phase Transitions in Coarse-Grained Lipid Bilayers," *J. Phys. Chem. B* **121**, 5770–5780 (2017).
- ³²G. Tiberio, L. Muccioli, R. Berardi, and C. Zannoni, "Towards in Silico Liquid Crystals. Realistic Transition Temperatures and Physical Properties for n-Cyanobiphenyls via Molecular Dynamics Simulations," *ChemPhysChem* **10**, 125–136 (2009).
- ³³Z. Zhang, O. G. Mouritsen, and M. J. Zuckermann, "Weak first-order orientational transition in the Lebwohl-Lasher model for liquid crystals," *Phys. Rev. Lett.* **69**, 2803–2806 (1992).
- ³⁴J. M. Fish and R. L. C. Vink, "Finite-size effects at first-order isotropic-to-nematic transitions," *Phys. Rev. B* **80**, 014107 (2009).
- ³⁵R. Shekhar, J. K. Whitmer, R. Malshe, J. A. Moreno-Razo, T. F. Roberts, and J. J. de Pablo, "Isotropic–nematic phase transition in the Lebwohl–Lasher model from density of states simulations," *J. Chem. Phys.* **136**, 234503 (2012).
- ³⁶M. Greschek and M. Schoen, "Finite-size scaling analysis of isotropic–nematic phase transitions in an anisometric Lennard-Jones fluid," *Phys. Rev. E* **83**, 011704 (2011).
- ³⁷H. Sidky, J. J. de Pablo, and J. K. Whitmer, "In Silico Measurement of Elastic Moduli of Nematic Liquid Crystals," *Phys. Rev. Lett.* **120**, 107801 (2018).
- ³⁸J. Shi, H. Sidky, and J. K. Whitmer, "Automated determination of n-cyanobiphenyl and n-cyanobiphenyl binary mixtures elastic constants in the nematic phase from molecular simulation," *Mol. Syst. Des. Eng.* **5**, 1131–1136 (2020).
- ³⁹J. K. Sheavly, J. I. Gold, M. Mavrikakis, and R. C. Van Lehn, "Molecular simulations of analyte partitioning and diffusion in liquid crystal sensors," *Mol. Syst. Des. Eng.* **151**, 362 (2020).
- ⁴⁰J. Zhang, J. Su, and H. Guo, "An Atomistic Simulation for 4-Cyano-4'-pentylbiphenyl and Its Homologue with a Reoptimized Force Field," *J. Phys. Chem. B* **115**, 2214–2227 (2011).
- ⁴¹J. Zhang, J. Su, Y. Ma, and H. Guo, "Coarse-Grained Molecular Dynamics Simulations of the Phase Behavior of the 4-Cyano-4'-pentylbiphenyl Liquid Crystal System," *J. Phys. Chem. B* **116**, 2075–2089 (2012).
- ⁴²J. Zhang and H. Guo, "Transferability of Coarse-Grained Force Field for nCB Liquid Crystal Systems," *J. Phys. Chem. B* **118**, 4647–4660 (2014).
- ⁴³S. Plimpton, "Fast parallel algorithms for short-range molecular dynamics," *J. Comput. Phys.* **117**, 1–19 (1995).
- ⁴⁴C. Zannoni, "Computer simulations," in *The molecular physics of liquid crystals*, edited by G. R. Luckhurst and C. Gray (Academic Press, London, 1979) pp. 191–220.
- ⁴⁵M. P. Allen and D. J. Tildesley, *Computer Simulation of Liquids*, 2nd ed. (Oxford University Press, Oxford, 2017).
- ⁴⁶R. Eppenga and D. Frenkel, "Monte Carlo study of the isotropic and nematic phases of infinitely thin hard platelets," *Mol. Phys.* **52**, 1303–1334 (2006).
- ⁴⁷K. Binder and D. P. Landau, "Finite-size scaling at first-order phase transitions," *Phys. Rev. B* **30**, 1477–1485 (1984).
- ⁴⁸K. Binder, "Applications of Monte Carlo methods to statistical physics," *Rep. Prog. Phys.* **60**, 487–559 (1997).
- ⁴⁹I. Haller, "Thermodynamic and static properties of liquid crystals," *Progress in Solid State Chemistry* **10**, 103–118 (1975).
- ⁵⁰I. Chirtoc, M. Chirtoc, C. Glorieux, and J. Thoen, "Determination of the order parameter and its critical exponent for nCB (n=5–8) liquid crystals from refractive index data," *Liq. Cryst.* **31**, 229–240 (2010).
- ⁵¹L. G. P. Dalmolen, S. J. Picken, A. F. de Jong, and W. H. de Jeu, "The order parameters and in nematic p-alkyl-p'-cyano-biphenyls: polarized Raman measurements and the influence of molecular association," *J. Phys. France* **46**, 1443–1449 (1984).
- ⁵²J. Deschamps, J. P. M. Trusler, and G. Jackson, "Vapor Pressure and Density of Thermotropic Liquid Crystals: MBBA, 5CB, and Novel Fluorinated Mesogens," *J. Phys. Chem. B* **112**, 3918–3926 (2008).
- ⁵³M. F. Palermo, A. Pizzirusso, L. Muccioli, and C. Zannoni, "An atomistic description of the nematic and smectic phases of 4-n-octyl-4'-cyanobiphenyl (8CB)," *J. Chem. Phys.* **138**, 204901 (2013).
- ⁵⁴K. Z. Takahashi, T. Aoyagi, and J.-i. Fukuda, "Multistep nucleation of anisotropic molecules," *Nat. Commun.* **12**, 5278 (2021).
- ⁵⁵J. Yoshida, S. Tamura, K. Hoshino, H. Yuge, H. Sato, A. Yamazaki, S. Yoneda, and G. Watanabe, "Comprehensive Understanding of Host- and Guest-Dependent Helix Inversion in Chiral Nematic Liquid Crystals: Experimental and Molecular Dynamics Simulation Study," *J. Phys. Chem. B* **122**, 10615–10626 (2018).
- ⁵⁶Y. Ishii, N. Matubayasi, G. Watanabe, T. Kato, and H. Washizu, "Molecular insights on confined water in the nanochannels of self-assembled ionic liquid crystal," *Sci. Adv.* **7**, eabf0669 (2021).